

Critical ultrasonic behavior near the normal-incommensurate phase transition in NaNO_2

J. Hu,* J. O. Fossum, C. W. Garland, and P. W. Wallace†

Department of Chemistry and Center for Materials Science and Engineering, Massachusetts Institute of Technology, Cambridge, Massachusetts 02139

(Received 2 December 1985)

The acoustic velocity and attenuation of the c_{22} longitudinal wave have been measured as a function of frequency (10–74 MHz) and temperature (165–180°C) in single-crystal sodium nitrite. Critical behavior in the high-temperature disordered (normal) phase near the normal-incommensurate phase transition can be well described in terms of a phenomenological dynamic-scaling theory. The static sound velocity exhibits a temperature dependence like that expected for the heat capacity. The velocity dispersion and the attenuation are well described with a critical relaxation time $\tau = (1.55 \times 10^{-11})t^{-1}$, where $t = (T - T_c)/T_c$. The velocity and attenuation exhibit the expected scaling behavior, and their ratio satisfies the Kramers-Kronig relation.

I. INTRODUCTION

The sodium nitrite crystal contains local dipole moments consisting of a NO_2^- ion and a nearest-neighbor Na^+ ion. The flipping of the NO_2^- ion in its double-minimum potential causes an associated displacement of the Na^+ ion. Since the dipoles have two possible orientations (parallel or antiparallel to the b axis), this system can be described in terms of an Ising pseudospin. However, NaNO_2 exhibits complex order-disorder phenomena since an incommensurate (antiferroelectric) phase exists over a narrow temperature range between the high-temperature paraelectric phase and the room-temperature ferroelectric phase.¹ The high-temperature "normal" phase is orthorhombic, space group $Immm$ (D_{2h}^{25}), and disordered with respect to the dipoles. On cooling, NaNO_2 undergoes a second-order transition at $T_c \approx 438.5$ K to an incommensurate phase with a sinusoidal modulation of the polarization. The incommensurate polarization wave in this phase is characterized by a wave vector $\mathbf{q}_s = \delta \mathbf{a}^*$, where $0.101 < \delta < 0.122$ with no lock-in at rational fractions like $\frac{1}{9}$.² On further cooling, there is a first-order transition at $T_1 \approx 437$ K into an ordered commensurate phase with space group $Im2m$ (C_{2v}^{20}).

We are concerned here with a detailed acoustic investigation of the critical behavior in the normal phase near the normal-incommensurate phase transition. Ultrasonic studies can provide information about both the static and dynamic critical behavior near second-order phase transitions. Indeed, a considerable amount is already known about the overall acoustic behavior of NaNO_2 from an extensive series of ultrasonic^{3–8} and Brillouin scattering^{9–10} studies. Hatta and co-workers^{4–7} have shown that longitudinal-acoustic waves in the normal phase are coupled to the order parameter Q via a quadratic term of the form

$$\sum_q \gamma_i(q) e_i(k) Q(q) Q(-q-k), \quad (1)$$

where $Q(q)$ and $\gamma_i(q)$ are Fourier transforms of $Q(\mathbf{r}_m)$ and the coupling constant $\gamma_i(\mathbf{r}_m - \mathbf{r}_n)$, and $e_i(k)$ is the

elastic strain associated with a longitudinal-acoustic mode with wave vector k propagating along the a , b , or c axis ($i=1-3$, respectively). The relative magnitudes of the coupling constants are $\gamma_1(q) : \gamma_2(q) : \gamma_3(q) = 1 : 2.7 : \sim 0$.⁷ Thus critical behavior associated with the c_{11} and c_{22} modes differs only in magnitude, and no critical behavior is observed for the c_{33} mode. Furthermore, none of the shear modes exhibit pretransitional behavior in the normal phase.⁴

The temperature dependence of the acoustic velocity and attenuation of the c_{22} longitudinal wave ($\mathbf{k} \parallel \mathbf{b}$) have been measured as a function of frequency with a phase-sensitive ultrasonic technique. The eQ^2 coupling gives rise to strong fluctuation damping of this acoustic mode, and critical relaxation behavior is observed near T_c . The experimental procedures are summarized briefly in Sec. II, the experimental results are presented in Sec. III, and the analysis of our data in terms of current theory for the critical dynamics of sound propagation¹¹ is given in Sec. IV. Section V contains a discussion of our results and a comparison with previous work.

II. EXPERIMENTAL PROCEDURES

Large single crystals of NaNO_2 , grown from the melt, were obtained from the Laboratoire de Physique Cristalline in Orsay, France. Two samples were used for acoustic measurements. Crystal *A* was light yellow in color and contained a few growth defects; the sample cut from this crystal did not contain visible defects and was used to characterize the overall behavior of the c_{22} wave over the range 150–180°C. Crystal *B* was almost colorless and was free from any visible defects; the sample cut from this crystal was used for all the detailed measurements in the disordered normal phase. Each sample had a pair of polished (010) surfaces that were flat and parallel to within ± 0.001 cm. The sample length in the [010] direction was 0.585 cm for sample *A* and 0.7765 cm for sample *B*.

A pulse-echo method was used at 10 MHz to determine the absolute ultrasonic velocity in the normal and com-

mensurate phases at temperatures far from T_c . Values of the attenuation and changes in the velocity were obtained as a function of temperature with a Matec MBS 8000 system, which provides for the coherent phase detection of two echo pulses.¹² Four sample-and-hold devices and a multiplexed 14-bit analog-to-digital converter provide digital output of the phase-detected signals. The system is controlled by a microcomputer which averages 100 readings and then calculates the attenuation and velocity. Since the signal-to-noise ratio is good for weak signals (~ 55 dB dynamic range), samples with large path lengths and well-separated echo pulses can be used.

Quartz transducers were used for measurements at 10.5 and 29.5 MHz, and lithium niobate transducers were used at 46.7 and 74.4 MHz. The transducers were bonded to the NaNO_2 sample with a very thin layer of Dow-Corning 200 silicone fluid. The sample holder was mounted in a large and well-regulated cylindrical oven, and the sample temperature was measured with a platinum resistance thermometer. The measurements on sample *A* were made during a very slow warming run: Typically a data point was taken after a wait of 30–60 min to ensure thermodynamic equilibrium, but a period of 1 day was necessary to achieve equilibrium when the sample went through the first-order commensurate-incommensurate transition. Measurements on sample *B* were made for both warming and cooling runs. In either case, at least 30 min was allowed for equilibration after changing the sample temperature (usually by a few tenths of a degree or less). Data presented at 10.5 MHz were obtained in three cooling and two warming runs; data at 29.5 MHz were obtained in one cooling and two warming runs. Since there were no systematic differences between data points from these warming and cooling scans, data at 46.7 and 74.4 MHz were taken only on cooling.

III. RESULTS

The temperature dependence on the LA [010] velocity v and attenuation α for sample *A* at 10 MHz shown in Fig. 1 over the range 165–176°C. Note that there is no pretransitional critical attenuation in the commensurate phase on approaching the commensurate-incommensurate transition at T_1 . The pretransitional behavior observed in the velocity just below T_1 is presumably due to the anomalous thermal expansion; the same type of velocity variation is observed for the shear modes which do not couple directly with the order parameter in any of the phases.⁴ The first-order discontinuity in v and α at T_1 is quite pronounced: $v_C - v_I = 114 \text{ m s}^{-1}$ and $\alpha_I - \alpha_C = 4.5 \text{ dB cm}^{-1}$. Substantial critical variations in v and α are observed near the second-order incommensurate-normal transition at T_c and over an appreciable range in the normal phase. The temperature-independent background attenuation $\alpha_0 \cong 2.3 \text{ dB cm}^{-1}$ is comparable to the values reported in Refs. 5 and 6. Such background attenuations, which are roughly independent of frequency,⁵ must be due to strains and defects in the NaNO_2 crystal rather than noncritical relaxation effects. Fortunately, α_0 was close to zero for all the runs carried out on sample *B* (see below).

The detailed variation of the [010] longitudinal velocity

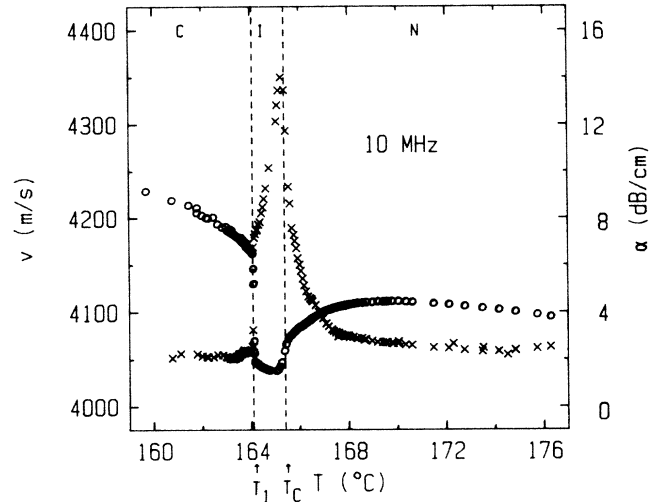


FIG. 1. Temperature dependence of the velocity v (\circ) and attenuation α (\times) of longitudinal ultrasonic waves propagating in the [010] direction. These measurements were made at 10 MHz on sample *A*. The temperatures of normal (*N*)-incommensurate (*I*) (T_c) and incommensurate (*I*)-commensurate (*C*) (T_1) transitions are indicated by the arrows.

as a function of frequency and temperature in the normal phase is shown in Fig. 2. Phase-detection data at all four frequencies were tied in with an absolute velocity of 4097 m s^{-1} at 175°C . This value is consistent with our pulse-echo velocity measurements at 10 MHz. The resulting 10-MHz (and 30-MHz) velocity of 4107.5 m s^{-1} at 170°C agrees well with a cluster of 170°C values in the (4000–4195)- m s^{-1} range for frequencies from 2.4 to 8.0 MHz, as reported by Hatta *et al.*⁵ The accuracy of the absolute velocity values given in Fig. 2 is not very high since our pulse-echo values had uncertainties of $\pm 80 \text{ m s}^{-1}$. However, this is not important for the analysis of critical velocity effects.

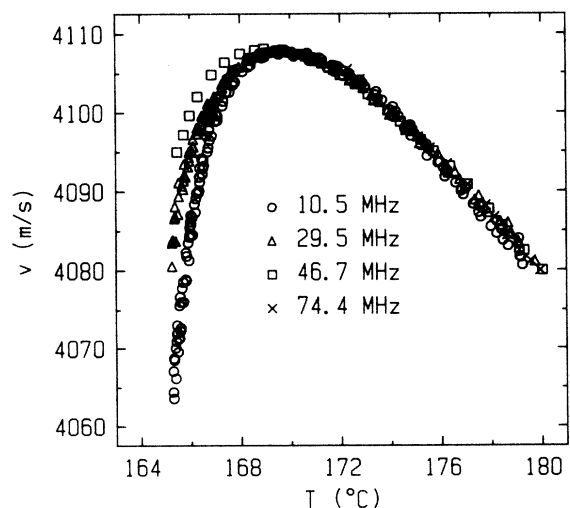


FIG. 2. Detailed [010] sound velocity variation in the disordered (normal) phase; these data were obtained on sample *B*.

The variation of the [010] longitudinal attenuation as a function of frequency and temperature in the normal phase is shown in Fig. 3. The quantity displayed is $\alpha/\omega^2 = (\alpha_{\text{obs}} - \alpha_0)/\omega^2$, where $\omega = 2\pi f$. The temperature-independent background attenuation α_0 is taken to be zero for runs at 47 and 74 MHz, but small α_0 values of about -0.7 and about $+1.0 \text{ dB cm}^{-1}$ have been assumed for the various 10- and 30-MHz runs, respectively. These choices lead to α/ω^2 values that are independent of frequency at temperatures far from T_c , as expected for relaxation processes when $\omega\tau \ll 1$.

It would also be of considerable interest to study the critical acoustic behavior near the normal-incommensurate transition as a function of the applied electric field E . The temperature range of the incommensurate phase stability, which is narrow even at $E=0$, decreases to zero at a triple point (critical end point) located at $\sim 438 \text{ K}$, $\sim 3.4 \text{ kV/cm}$.¹³ An attempt was made to carry out such an investigation with our present NaNO_2 samples. Unfortunately, the resistivity of NaNO_2 decreases markedly as the crystal is heated above the normal-incommensurate transition temperature. As a result, there was considerable Joule self-heating which gave rise to a substantial temperature gradient within our rather large crystals. This made it impossible to carry out well-characterized acoustic measurements in the presence of an applied field of even 1 kV/cm .

IV. ANALYSIS OF DATA

A. Review of theory

The critical behavior of the acoustic velocity and attenuation can be described with a phenomenological theory based on linear-response theory and dynamic scaling.¹¹ One starts from a complex, frequency-dependent elastic stiffness constant $\tilde{c}(\omega, T)$ which can be written in the form

$$\tilde{c} = c_0 + \Delta c, \quad (2)$$

where $c_0 = \rho v_0^2$ is the bare stiffness (i.e., the elastic constant in the absence of any coupling between strain and the order parameter) and Δc is the complex critical contribution. The quantity Δc contains information about the critical temperature dependence of the static velocity $v(\omega=0)$ as well as the frequency and temperature dependence of the critical attenuation $\Delta\alpha(\omega)$ and the critical velocity dispersion $v(\omega) - v(0)$. ρ is the mass density and $v_0(T)$ is the bare sound velocity.

From Eq. (2) one obtains

$$\rho(v^2 - v_0^2) = \text{Re}\Delta c, \quad (3)$$

$$2\rho v^3 \Delta\alpha/\omega = -\text{Im}\Delta c. \quad (4)$$

When the quantity $\Delta v = v_0 - v$ is small, Eq. (3) can be rewritten in the convenient form

$$2\rho\bar{v}\Delta v \cong -\text{Re}\Delta c, \quad (5)$$

where $\bar{v} = (v + v_0)/2 \cong \text{const}$. Using the dynamic scaling form given by Fossum¹¹ for Δc in the case of eQ^2 quadratic coupling, we find

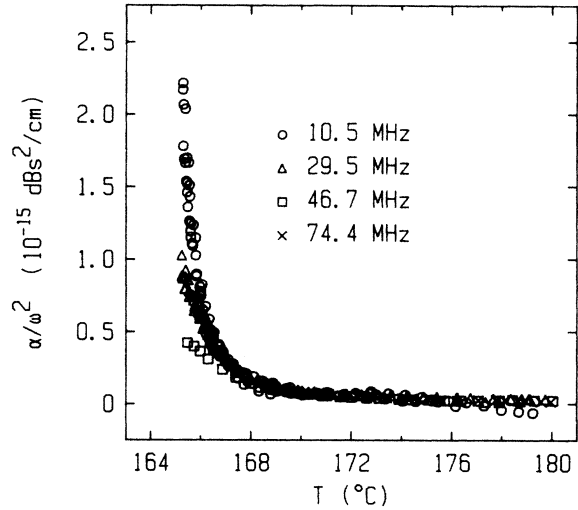


FIG. 3. Detailed [010] attenuation variation in the disordered (normal) phase; these data were obtained on sample B.

$$\bar{v}\Delta v = At^{-\mu}(1 + Dt^{0.5})G(\omega\tau), \quad (6)$$

$$v^3\Delta\alpha/\omega = (\mu/zv)At^{-\mu}(1 + Dt^{0.5})\omega\tau F(\omega\tau), \quad (7)$$

where $t \equiv (T - T_c)/T_c$ is the reduced temperature, μ is a static critical exponent (see Ref. 11 for details), and $\tau = \tau_0 t^{-z\nu}$ is the critical relaxation time. (z is the dynamic critical exponent defined by $\tau \sim \xi^z$, where $\xi = \xi_0 t^{-\nu}$ is the correlation length.) The functions $G(\omega\tau)$ and $F(\omega\tau)$ are defined by

$$G(\omega\tau) = \cos \left[\frac{\mu}{z\nu} \arctan(\omega\tau) \right] [\cos \arctan(\omega\tau)]^{\mu/z\nu}, \quad (8)$$

$$F(\omega\tau) = \frac{z\nu}{\mu} \frac{1}{\omega\tau} \sin \left[\frac{\mu}{z\nu} \arctan(\omega\tau) \right] [\cos \arctan(\omega\tau)]^{\mu/z\nu}. \quad (9)$$

In the limit $\omega\tau \ll 1$,

$$G(\omega\tau \ll 1) = F(\omega\tau \ll 1) = 1, \quad (10)$$

and in the opposite limit $\omega\tau \gg 1$,

$$G(\omega\tau \gg 1) = \cos \left[\frac{\pi}{2} \frac{\mu}{z\nu} \right] (\omega\tau)^{-\mu/z\nu}, \quad (11)$$

$$F(\omega\tau \gg 1) = \frac{z\nu}{\mu} \sin \left[\frac{\pi}{2} \frac{\mu}{z\nu} \right] (\omega\tau)^{-(1+\mu/z\nu)}. \quad (12)$$

The general forms of $F(\omega\tau)$ and $G(\omega\tau)$ given in Eqs. (8) and (9) represent empirical functions that provide a smooth crossover between the asymptotic $\omega\tau \ll 1$ and $\omega\tau \gg 1$ limits.¹⁴ It should be noted that Eqs. (6) and (7) automatically satisfy the Kramers-Kronig relations. Since the treatment given in Ref. 11 is phenomenological, the critical exponents μ and $z\nu$ can be viewed as effective values describing the range of data fitted and may differ from the expected asymptotic values.

For data obtained in the limiting region $\omega\tau \ll 1$ (low ω and large ΔT), we will use

$$\Delta v = A_1 t^{-\mu} (1 + Dt^{0.5}) \quad (13)$$

and

$$\Delta\alpha/\omega^2 = \frac{\mu}{z\nu} \frac{A}{v^3} t^{-\mu} (1 + Dt^{0.5})\tau \quad (14a)$$

$$= A_2 t^{-(\mu+z\nu)} (1 + Dt^{0.5}), \quad (14b)$$

where $A_1 \equiv A/\bar{v}$ and $A_2 \equiv \mu\tau_0 A/z\nu v^3$ can be taken as constants since $\bar{v} = 4070 \text{ m s}^{-1}$ within $\pm 60 \text{ m s}^{-1}$ and $v^3 = 6.82 \times 10^{10} \text{ m}^3 \text{ s}^{-3}$ within $\pm 0.11 \times 10^{10} \text{ m}^3 \text{ s}^{-3}$ over the investigated range of ω and T . For a non-symmetry-breaking strain like the c_{22} longitudinal mode in an orthorhombic crystal, one expects the static Δv to vary like the heat capacity.^{11,15} Thus the exponent μ should be the critical heat-capacity exponent α and a correction-to-scaling term should appear as in the case of C_p . We have extended the treatment of Ref. 11 by including the correction-to-scaling term Dt^{Δ_1} with the critical exponent Δ_1 taken to be 0.5, which is its theoretical value.¹⁶ Note that Eq. (13) appears to give a divergence in Δv (and thus a negative velocity) at T_c , which is not physically correct. In principle, one should consider the critical behavior of the bulk compliance near T_c ; however, the form given in Eq. (13) is valid as long as $\Delta v/v_0 \ll 1$. In the case of NaNO_2 , it will be shown below that the maximum value of $\Delta v/v_0 \approx 0.036$. Note also that Eq. (14a) corresponds to the well-known form¹⁷ $\Delta\alpha \sim t^{-\mu}\omega^2\tau$, except that a correction-to-scaling term $Dt^{0.5}$ appears. It will be seen that our NaNO_2 data require such a theoretically expected correction-to-scaling term.

Let us now define the Kramers-Kronig ratio R by

$$R \equiv \frac{1}{\omega} \frac{\text{Im}\Delta c}{\text{Re}\Delta c}. \quad (15)$$

It follows from Eqs. (4) and (5) that

$$R = \frac{v^3 \Delta\alpha/\omega^2}{\bar{v}\Delta v}, \quad (16)$$

where $\Delta\alpha$ should be expressed in Np m^{-1} (experimental $\Delta\alpha$ values in dB cm^{-1} must be multiplied by $100/8.686 = 11.51$). In determining the experimental value of R with Eq. (16), we will take into account the weak temperature and frequency dependence of both v^3 and \bar{v} . The theoretical behavior of R is obtained by substituting Eqs. (6) and (7) into Eq. (16):

$$R = \frac{\mu}{z\nu} \tau \frac{F(\omega\tau)}{G(\omega\tau)}. \quad (17)$$

This has the following limiting values:

$$R \rightarrow \mu\tau/z\nu \text{ for } \omega\tau \ll 1 \quad (18a)$$

$$\rightarrow \pi\mu/2z\nu\omega \text{ for } \omega\tau \gg 1. \quad (18b)$$

Finally, we give scaling forms for the velocity, the attenuation, and the Kramers-Kronig ratio:

$$\Delta v/\Delta v(\omega\tau \ll 1) = G(\omega\tau), \quad (19)$$

$$\Delta\alpha/\Delta\alpha(\omega\tau \ll 1) = F(\omega\tau), \quad (20)$$

$$(z\nu/\mu)\omega R = \omega\tau F(\omega\tau)/G(\omega\tau). \quad (21)$$

B. Fitting of data

Before the NaNO_2 data can be analyzed in terms of the theoretical expressions given in Sec. IV A, it is necessary to establish the temperature-dependent bare velocity $v_0(T)$. Figure 4 shows a superposition of our static velocity data with those obtained from Ref. 5. Static velocity data consist of all the velocity values that do not exhibit frequency dispersion, i.e., values of $v(\omega, T)$ that equal $v(0, T)$ at any given temperature T . The data points taken from Hatta *et al.*⁵ have been shifted by -92 m s^{-1} and -1.0 K in order to correct for different absolute velocity values and different T_c values for sample *B* and the sample used in their work. Comparable shifts in v and T_c occur between the data in Refs. 4 and 5, and the T_c values for our samples *A* and *B* differ by 0.15 K .

Two choices of $v_0(T)$ are shown in Fig. 4. In both cases a linear variation is assumed: Line *a* is a visual fit to the experimental points over the range $220\text{--}230^\circ\text{C}$, while line *b* is the best least-squares line through the data points over the range $210\text{--}230^\circ\text{C}$. If the bare velocity is expressed in the form

$$v_0(T) = v_0(438.4 \text{ K}) - S(T - 438.4 \text{ K}), \quad (22)$$

then $v_0(438.4 \text{ K}) = 4233.56 \text{ m s}^{-1}$ and the slope $S = 6.50 \text{ m s}^{-1} \text{ K}^{-1}$ for line *a*, while $v_0(438.4 \text{ K}) = 4198.21 \text{ m s}^{-1}$ and $S = 5.927 \text{ m s}^{-1} \text{ K}^{-1}$ for line *b*. We consider line *a* to be the more plausible choice for $v_0(T)$ but will explore the consequences of both choices.

Figure 5 shows the dependence of $\Delta v(\omega, T) = v_0(T) - v(\omega, T)$ on $\Delta T = T - T_c$ when $v_0(T)$ is represented by line *a*. The value of T_c was taken to be $165.25^\circ\text{C} = 438.4 \text{ K}$, which is 0.1 K above the temperature when $\alpha(10 \text{ MHz})$ achieves its maximum value. This choice is consistent with the conclusions drawn from extensive heat-capacity, dielectric, and ultrasonic data reported by Hatta *et al.*^{4,5} The curve labeled $\omega\tau \ll 1$ in Fig. 5 represents a least-squares fit of the static values of Δv with Eq. (13); the resulting parameters μ , A_1 , and D (as well as $A = A_1\bar{v}$) are those of fit 1 in Table I. Note that the value 0.116 for μ is very close to the Ising heat-capacity exponent ($\alpha_I = 0.11$). If $v_0(T)$ is represented by line *b* in Fig. 4, the values of Δv are, of course, modified, but an equally good fit to the static Δv values can be achieved. This alternate set of parameters μ , A , and D is given in fit 2 of Table I. Note that the exponent μ increases to 0.164 . We have also tested the effect of changing T_c to 438.3 K , which corresponds to the temperature of maximum attenuation at 10 MHz and is thus the lowest possible value for T_c . The resulting μ , A , and D parameter values are given in fits 3 and 4 of Table I. Even this unrealistically large change in T_c has very little effect on the parameter values. Since fits 1–4 give almost identical χ^2_ν values (0.95 to 1.00) for fitting Δv with Eq. (13), there is no statistical basis for choosing one in prefer-

TABLE I. Parameter values obtained from fitting the limiting ($\omega\tau \ll 1$) critical velocity and attenuation data with Eqs. (13) and (14). The bare velocity choices (a and b) are shown in Fig. 4 and described with Eq. (22). The χ^2_ν values indicate the quality of the fit to $\Delta\alpha/\omega^2$ with the indicated τ_0 and $z\nu$ when μ , A , and D are held fixed at the values obtained from the velocity fit.

Fit	v_0	T_c (K)	μ	A ($10^5 \text{ m}^2 \text{ s}^{-2}$)	D	$z\nu$	τ_0 (10^{-11} s)	χ^2_ν	A_1 (m s^{-1})	A_2 ($10^{-19} \text{ dB s}^2 \text{ cm}^{-1}$)
1	a	438.4	0.116	3.162	-2.657	1.02	1.412	1.47	77.69	6.596
2	b	438.4	0.164	1.817	-3.229	0.93	2.549	1.45	44.65	9.441
3	a	438.3	0.127	2.998	-2.596	1.07	0.897	1.46	73.65	4.668
4	b	438.3	0.179	1.695	-3.163	0.96	1.868	1.44	41.65	7.368
5	a	438.4	0.116	3.162	-2.657	1.0	1.549	1.47	77.69	7.393
6	a	438.4	0.116	3.162	-2.657	1.28	0.435	2.30	77.69	1.614

ence to another. However, fit 1 is based on the most physically reasonable choice of v_0 and T_c .

Note that curves representing the frequency dispersion predicted when $\omega\tau$ is not negligible are also shown in Fig. 5. These were obtained with Eq. (6) using relaxation times τ obtained below from fitting the critical attenuation data.

The critical contribution to the attenuation is given by

$$\Delta\alpha/\omega^2 = \alpha/\omega^2 - \alpha_{nc}/\omega^2, \quad (23)$$

where α_{nc}/ω^2 is a frequency- and temperature-independent quantity which represents any noncritical relaxation contributions to the attenuation. A least-squares fit to those attenuation data for which $\omega\tau \ll 1$ was carried out using Eqs. (14a) and (23) with τ_0 , $z\nu$, and α_{nc} as adjustable parameters. The resulting value of α_{nc}/ω^2 was $0.46 \times 10^{-17} \text{ dB s}^2 \text{ cm}^{-1}$, which is quite small compared with observed α/ω^2 values that range from 2×10^{-17} to 220×10^{-17} . The parameters μ , A , and D that appear in Eq. (14a) were fixed at the values obtained from the velocity fit. The least-squares values of $z\nu$ and τ_0 (and for convenience A_2) are given in Table I for both choices of $v_0(T)$ and T_c .

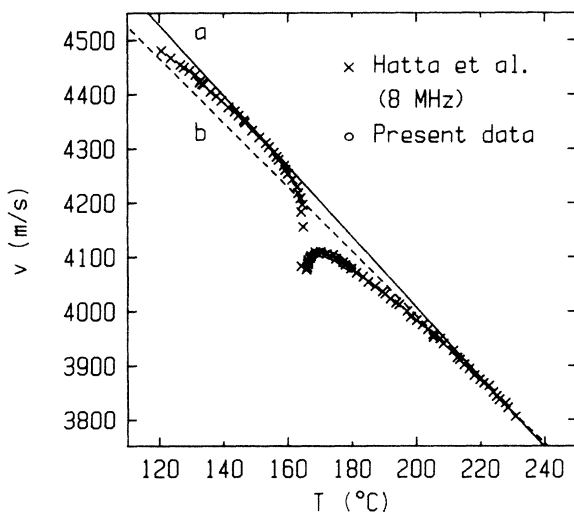


FIG. 4. Sound velocity of [010] longitudinal waves over a wide temperature range obtained from Ref. 5. These 8-MHz points have been shifted to match our static velocity data (see text). Two choices for the bare velocity $v_0(T)$ are shown by the solid and dashed lines.

The least-squares value of the exponent $z\nu$ obtained from fits 1–4 summarized in Table I is 1.00 ± 0.07 . This value corresponds to the conventional Van Hove value rather than the critical value $z\nu = 1.28$ expected for a three-dimensional (3D) Ising model or $z\nu = 1.36$ for a 3D XY model.¹⁸ In order to compare the quality of attenuation fits that can be obtained with conventional and Ising-like dynamic critical behavior, we have carried out fits with $z\nu$ fixed at 1.00 (fit 5) and $z\nu$ fixed at 1.28 (fit 6). The resulting τ_0 (and A_2) values are given in Table I. Figure 6 shows the variation of $\Delta\alpha/\omega^2$ with ΔT . The solid and dashed lines represent the fits obtained with $z\nu = 1.00$ (fit 5) and 1.28 (fit 6), respectively. The low-frequency limiting lines (labeled $\omega\tau \ll 1$) were obtained from the least-squares fits with Eq. (14a); the finite $\omega\tau$ curves were calculated from Eq. (7) with no further adjustment of the parameters.

The temperature dependence of the Kramers-Kronig ratio [see Eq. (16)] is shown in Fig. 7. As indicated by Eqs. (18a) and (18b), this quantity provides a direct evaluation of $\mu/z\nu$ and of the τ values at large ΔT . The

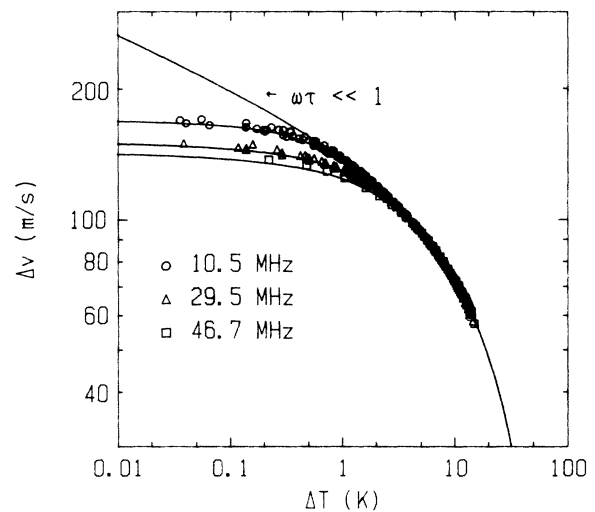


FIG. 5. Critical velocity contribution $\Delta v = v_0(T) - v(\omega, T)$ as a function of $\Delta T = T - T_c$. Line a in Fig. 4 was used for the bare velocity v_0 , and $T_c = 165.25^\circ\text{C} = 438.40 \text{ K}$. The static limit ($\omega\tau \ll 1$) curve was obtained from a least-squares fit with Eq. (13). The curves for 10.5, 29.5, and 46.7 MHz were calculated from Eq. (6) using relaxation times $\tau = (1.55 \times 10^{-11})t^{-1}$ obtained from fitting the attenuation.

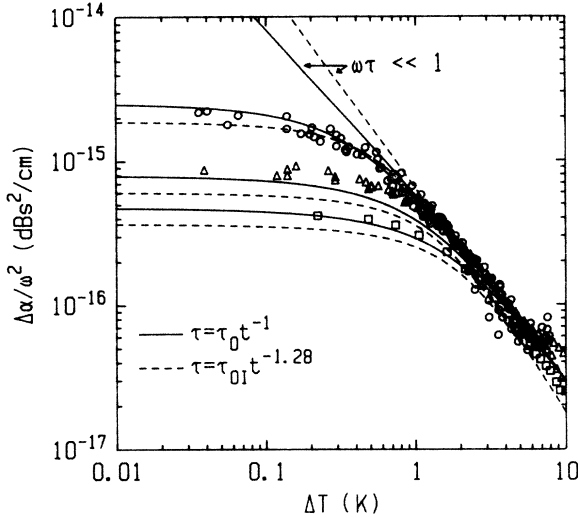


FIG. 6. Critical attenuation $\Delta\alpha$ as a function of ΔT . Data are shown at 10.5 MHz (\circ), 29.5 MHz (\triangle), and 46.7 MHz (\square). In the large- ΔT , small- ω regime where $\Delta\alpha$ is proportional to ω^2 , a least-squares fit was carried out with Eq. (14a). The finite-frequency curves were calculated from Eq. (7) with no further adjustment of the fitting parameters.

theoretical curves given in Fig. 7 are based on Eq. (17) with $\mu/z\nu=0.116$, $\tau_0=1.55\times 10^{-11}$ s, and $z\nu=1.0$. These parameters values were obtained from our previous fit 5 to the limiting $\Delta\alpha/\omega^2$ values ($\omega\tau\ll 1$ regime corresponding to large ΔT). The good agreement between theory and experiment in Fig. 7 confirms the τ values obtained from Eq. (14a) and shows that experimental data close to T_c are consistent with $\mu/z\nu=0.116$. These conclusions are independent of the form $At^{-\mu}(1+Dt^{0.5})$ used in Eqs. (13) and (14a) to represent the temperature dependence of the static velocity and the relaxation strength.

Finally, we present scaling plots for the critical velocity, the critical attenuation, and the Kramers-Kronig ratio in Figs. 8–10. In all these plots, the theoretical curve is based on $\mu/z\nu=0.116$ and $\tau=(1.55\times 10^{-10})t^{-1}$ sec.

We have also tested the possibility of fitting our static Δv data with a negative μ value, which would correspond to the heat capacity exhibiting a finite cusp. Good fits can, indeed, be achieved with μ fixed at -0.026 when background b is used:

$$\Delta v = 1074.0 - 1138.0t^{0.026} \quad (24)$$

However, this representation of the static behavior does not change at all the values of $z\nu$ inferred from the attenuation and dispersion data.

V. DISCUSSION

The theoretical analysis of Cowley and Bruce¹⁹ predicts that critical behavior at the normal-incommensurate transition should correspond to that for the three-dimensional XY ($d=3$, $n=2$) universality class. This would lead to $\mu=\alpha_{XY}\simeq -0.026$ and $z\nu=1.36$. However, Hatta *et al.*^{5,6} have extended the Cowley-Bruce theory to provide an explicit treatment of the critical behavior of long-wave

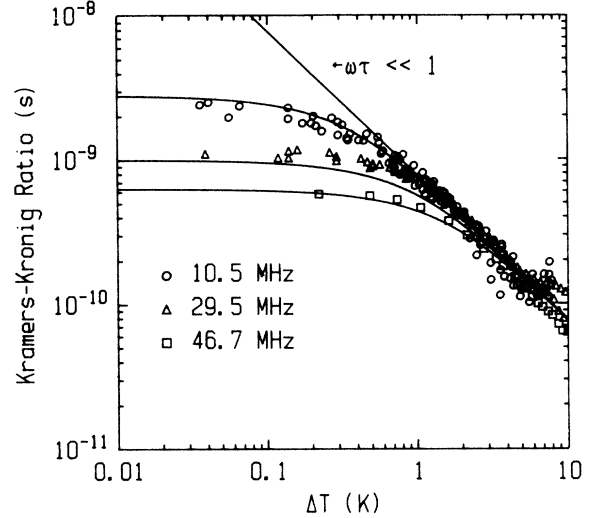


FIG. 7. Temperature variation of the Kramers-Kronig ratio defined by Eq. (16). The smooth curves represent the theoretical form given in Eq. (17) using the parameters of fit 5 in Table I.

acoustic modes in NaNO_2 . They show that in the incommensurate phase longitudinal acoustic waves with wave vector $k\equiv 0$ couple with the amplitude fluctuation modes but not the phase fluctuation modes. The critical fluctuation contribution in the normal phase, which arises from the coupling given in Eq. (1), is also dominated by amplitude fluctuations. Thus one might expect Ising ($d=3$, $n=1$) universal behavior, as discussed by Hatta,⁴⁻⁷ which would yield $\mu=\alpha_I=0.11$ and $z\nu=1.28$.

Our static velocity data [i.e., $v(\omega, T)$ points for which $\omega\tau\ll 1$] are consistent with a small critical exponent μ , but the range of these data is too limited to distinguish between $\mu=+0.11$ and -0.03 . High-resolution velocity data obtained at a frequency of 100 kHz or lower are needed to resolve the static critical behavior of the acoustic properties.

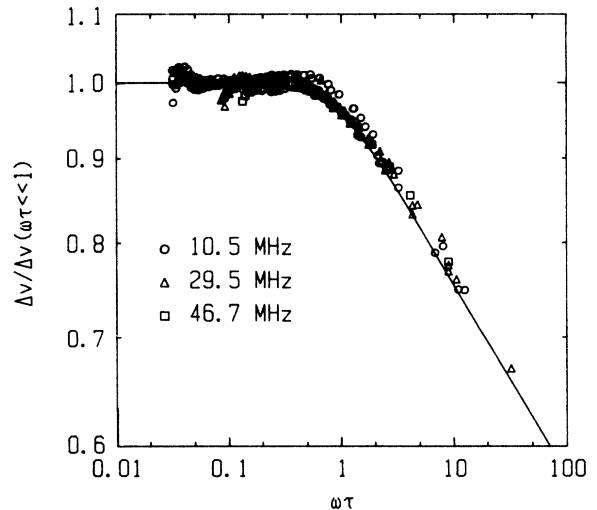


FIG. 8. Scaling plot for the critical velocity. The curve represents $G(\omega\tau)$ defined in Eq. (8).

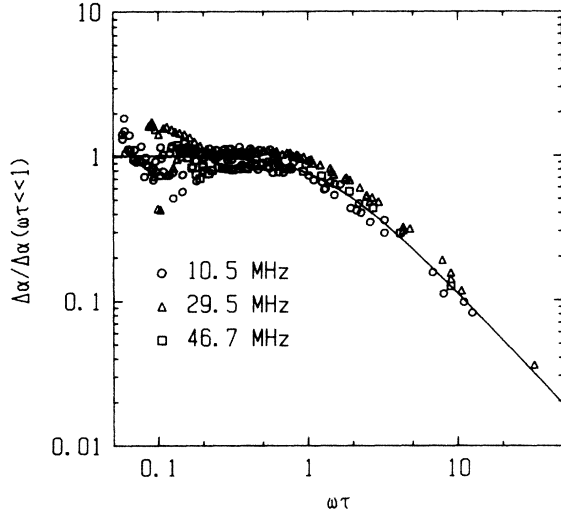


FIG. 9. Scaling plot for the critical attenuation. The curve represents $F(\omega\tau)$ defined in Eq. (9).

Direct measurements of the heat capacity²⁰ indicate that the critical exponent α is positive. There may, however, be complications associated with the analysis of the C_p data since correction-to-scaling terms were not used and scaling was not obeyed ($\alpha=0.38$ was reported for $T > T_c$ and $\alpha'=0.18$ was reported for $T < T_c$).²⁰ The present acoustic data are consistent with $-0.03 \leq \mu \leq 0.18$, but they are not consistent with a μ value as large as 0.38. If μ is fixed at 0.38 and the bare velocity line is taken to be adjustable, a completely artificial fit is obtained with Eqs. (13) and (22). In particular, $v_0(438.4 \text{ K}) = 3967.12 \text{ m s}^{-1}$ and $D = -146.96$, which means that the $v_0(T)$ line lies below the observed $v(T)$ values and a negative correction-to-scaling term dominates the positive “leading singularity” at almost all temperatures (i.e., for $\Delta T \geq 0.02 \text{ K}$).

The experimental data require a $z\nu$ value that is much closer to 1.0 than either the Ising (1.28) or the XY (1.36) values. These theoretical values of $z\nu$ correspond to those obtained with model A of Hohenberg and Halperin.¹⁸ This time-dependent Ginzburg-Landau model for a single n -component order parameter is a purely relaxational model in which no quantities are conserved and should be an appropriate model for NaNO_2 . A direct comparison between the fits with $z\nu=1.0$ and 1.28 is given in Fig. 6. The $\Delta\alpha/\omega^2$ data far from T_c require that $\mu+z\nu \approx 1.1$, which implies that $z\nu \leq 1.1$ for large t values. Close to T_c , the value $z\nu=1.28$ is clearly too large since it leads to systematic errors in the magnitude and temperature dependence of the critical attenuation and critical dispersion at finite frequencies. Our conclusion that $z\nu \approx 1.0$ is consistent with Hatta’s analysis of his attenuation data,⁶ which is based on the assumption that $z\nu=1$. It is also qualitatively supported by the results of Esaya *et al.*,⁸ who reported $z\nu=0.8$. Note also that the values of $z\nu$ are fairly insensitive to possible choice of bare velocity or critical temperature. Table I shows that $z\nu=1.00 \pm 0.07$ for two plausible choices of v_0 and two limiting choices of T_c .

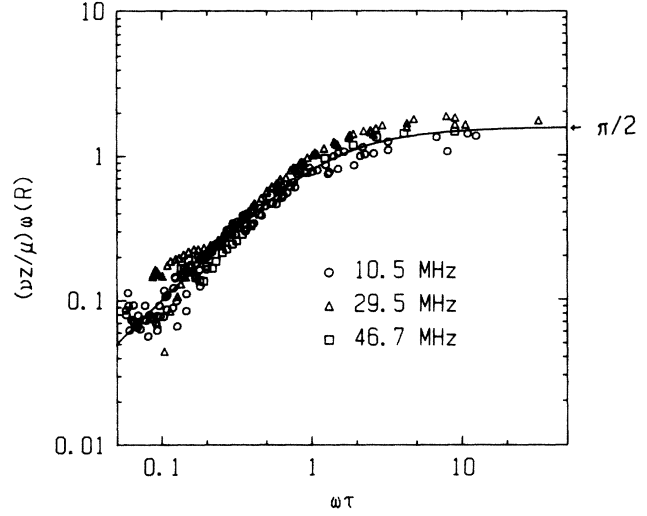


FIG. 10. Scaling plot for the quantity $(z\nu/\mu)\omega R$, where R is the Kramers-Kronig ratio, using $z\nu/\mu=1/0.116=8.62$. The limiting theoretical values for this quantity are $\omega\tau$ when $\omega\tau \ll 1$ and $\pi/2$ when $\omega\tau \gg 1$.

Hatta and co-workers⁵⁻⁶ have measured the longitudinal attenuation in both the incommensurate and normal phases. In the incommensurate phase, there is a linear coupling between the amplitude fluctuations and the acoustic phonons which gives rise to Landau-Khalatnikov-type damping below T_c . The relaxation time for this coupled longitudinal-amplitude mode was found to show conventional critical behavior,

$$\tau_A = 4.4 \times 10^{-12} |t|^{-1}, \quad (25)$$

in the incommensurate phase.⁷ The analysis of Hatta’s attenuation data in the normal phase⁶ is based on the assumption that τ is equal to τ_A and the use of the following empirical scaling function:

$$\frac{\Delta\alpha(T)}{\Delta\alpha(T_c)} = f(\omega\tau) = \frac{(\omega\tau)^{1+y}}{c + (\omega\tau)^{1+y}}. \quad (26)$$

The resulting values of the fitting parameters were $y=0.13 \pm 0.05$ and $c=0.103 \pm 0.002$.⁶ Equation (26) was obtained from a scaling form $\Delta\alpha = B\omega^{1-y}f(\omega\tau)$ which gives the limiting expressions

$$\Delta\alpha(T_c) = B\omega^{1-y}, \quad (27a)$$

$$\Delta\alpha(\omega\tau \ll 1) = (B/c)\omega^2\tau^{1+y}. \quad (27b)$$

Comparison of these expressions with those obtained from our theoretical analysis yields the following equivalences:

$$y = \frac{\mu}{z\nu}, \quad B = \pi A_2 / 2\tau_0^{1+\mu/z\nu}, \quad (28)$$

and

$$c = \frac{\pi}{2(1+Dt^{0.5})} \left[\frac{\tau_{0H}}{\tau_0} \right]^{1+\mu/z\nu}, \quad (29)$$

where $\tau_{0H} = 4.4 \times 10^{-12}$ and our $\tau_0 = 1.55 \times 10^{-11}$. Using our parameters from fit 5, one finds that $\mu/z\nu = 0.12$,

$B = 1.345 \times 10^{-6} \text{ dB cm}^{-1} \text{ s}^{0.88}$, and $c = 0.39 - 0.58$ for $\Delta T = 0 - 7 \text{ K}$. Thus agreement between Hatta's γ value and our $\mu/z\nu$ value is excellent, but the Hatta value of c disagrees substantially with the average value obtained from Eq. (29).

A more direct comparison between our theoretical dynamic scaling expressions and Hatta's velocity and attenuation data^{4,5,21} is given in Figs. 11 and 12. In Fig. 11, the velocity variations at 6.3 (Ref. 4) and 8.0 MHz (Ref. 5) are compared with the theoretical curve obtained with Eqs. (13) and (22) using the parameter values from fit 5. These data by Hatta *et al.* have been shifted to coincide with our static velocity data (which lie in the range 165–180°C). The shifts were -265 m s^{-1} and $+0.3 \text{ K}$ for the 6.3-MHz points and -92 m s^{-1} and -1.0 K for the 8.0-MHz points. Such shifts have no effect on the shape of the velocity variation, which is the feature that is being tested. Figure 11 shows that Eq. (13) with parameters chosen to represent the temperature dependence of our static velocity over a relatively narrow range provides an excellent description of the temperature dependence of Hatta's static velocity over quite a wide temperature range. In Fig. 12, the critical attenuation observed by Hatta^{5,21} at 4.35 and 9.0 MHz is compared with the theoretical curves obtained from Eq. (7) using the parameter values from fit 5. The overall agreement between Hatta's critical attenuation data and our theoretical lines is quite good although these experimental values close to T_c are systematically larger (by 10–15%) than the predicted values. Thus Figs. 11 and 12 show that the equations and parameter values used in describing our own data also provide a good description of Hatta's critical data.

It should be noted that the critical relaxation times given by our result,

$$\tau = (1.55 \times 10^{-11}) t^{-1}, \quad (30)$$

are much longer than the correlation time associated with the flipping of an individual NO_2^- ion. An analysis of high-resolution inelastic-neutron-scattering data at 200°C gives a flipping time of approximately $5 \times 10^{-11} \text{ s}$.² The cooperative relaxation times range from $6.79 \times 10^{-8} \text{ s}$ at 166.25°C ($\Delta T = 0.1$) to $1.95 \times 10^{-10} \text{ s}$ at 200°C ($\Delta T = 34.75$) if one assumes that Eq. (30) is valid that far from T_c . It is also of interest to compare the acoustic relaxation times with those obtained from dielectric-loss measurements.²² The polarization relaxation times τ_p were calculated from $\epsilon''(\omega)$ data at 3 and 5 MHz using a Debye single-relaxation formalism. The $1/\tau_p$ values shown in Fig. 3 of Ref. 22 show a slightly nonlinear dependence on $\Delta T = T - T_c$ for $\Delta T > 2 \text{ K}$ and a distinct curvature close to T_c leading to a nonzero value of $1.36 \times 10^8 \text{ s}^{-1}$ (i.e., $\tau_p = 7.33 \times 10^{-9} \text{ s}$) at T_c . The latter feature of the τ_p behavior is clearly different from the acoustic τ behavior, since our attenuation and velocity dispersion close to T_c require rapidly varying τ values that are 10–100 times larger than the reported $\tau_p(\text{max})$ value. It should be noted, however, that the τ_p values over the range $\Delta T = 3 - 12 \text{ K}$ can be well represented by $\tau_p = (1.86 \times 10^{-11}) t^{-1}$, in reasonable agreement with the magnitude of our acoustic τ values. The exact relationship between τ_p and the

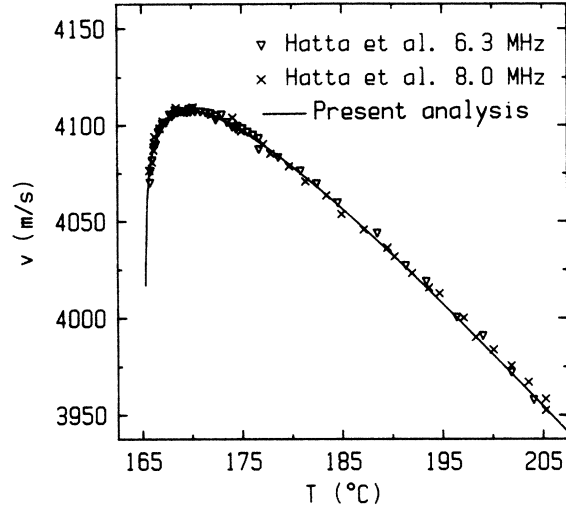


FIG. 11. Comparison of the static velocity variation reported by Hatta (Refs. 4 and 5) with the theoretical curve representing our present analysis (see the text).

order-parameter relaxation time τ obtained from acoustic measurements is not clear.

In conclusion, we have measured both the static and dynamic behavior of the c_{22} longitudinal mode in NaNO_2 . The critical velocity and attenuation behavior near the normal-incommensurate transition are well described by dynamic-scaling expressions. The static (i.e., $\omega\tau \ll 1$) velocity shows a temperature dependence analogous to that expected for the heat capacity. The present data are consistent with either Ising or XY behavior: The critical exponent μ lies in the range -0.03 to $+0.18$ and could agree with either $\alpha_{XY} = -0.026$ or $\alpha_I = 0.11$. We feel that the Ising fit is somewhat better overall, but new low-frequency experiments are needed to resolve this question. The critical relaxation time is characterized by the dynamic exponent $z\nu = 1.00 \pm 0.07$, which corresponds to conventional critical slowing down. Both the velocity

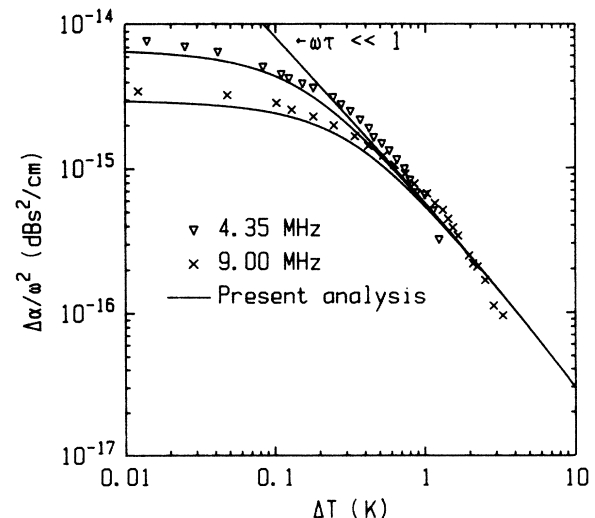


FIG. 12. Comparison of the critical attenuation reported by Hatta (Refs. 5 and 21) with the theoretical curves calculated with Eq. (7).

dispersion and the attenuation over a wide range of frequencies and reduced temperatures are well represented by our theoretical model. In particular, the data are analyzed in a self-consistent manner so that the Kramer-Kronig relation is satisfied, and both velocity and attenuation exhibit the expected scaling behavior.

ACKNOWLEDGMENTS

We wish to thank J. P. Chappelle for providing two high-quality single crystals of NaNO_2 . This work was supported by the National Science Foundation under Contract No. CHE-84-00982.

*Present address: Department of Physics, Queen's University, Kingston, Canada K7U 3N6.

†Present address: E. I. Dupont de Nemours and Co., Inc., P.O. Box 13999 Research Triangle Park, NC 27709.

¹Y. Yamada and T. Yamada, *J. Phys. Soc. Jpn.* **21**, 2167 (1966); V. Heine, R. M. Lynden-Bell, J. Desmond, C. McConnell, and I. R. McDonald, *Z. Phys. B* **56**, 229 (1984).

²D. Durand, F. Denoyer, M. Lambert, L. Bernard, and R. Currat, *J. Phys. (Paris)* **43**, 149 (1982), and references cited therein.

³K. Hamano and K. Ema, *J. Phys. Soc. Jpn.* **45**, 923 (1978).

⁴I. Hatta, Y. Shimizu, and K. Hamano, *J. Phys. Soc. Jpn.* **44**, 1887 (1978), and references cited therein.

⁵I. Hatta, M. Hanami, and K. Hamano, *J. Phys. Soc. Jpn.* **48**, 160 (1980).

⁶I. Hatta, *J. Phys. Soc. Jpn.* **49**, 163 (1980).

⁷I. Hatta, *J. Phys. Soc. Jpn.* **53**, 635 (1984).

⁸S. K. Esayan, V. V. Lemanov, and N. Mamatkulov, *Fiz. Tverd. Tela (Leningrad)* **23**, 2048 (1981) [*Sov. Phys.—Solid State* **23**, 1195 (1981)].

⁹H. Shimizu, M. Tsukamoto, Y. Ishibashi, and M. Umeno, *J. Phys. Soc. Jpn.* **36**, 498 (1974).

¹⁰T. Yagi, Y. Hidako, and K. Miura, *J. Phys. Soc. Jpn.* **51**, 3562

(1982).

¹¹J. O. Fossum, *J. Phys. C* **18**, 5531 (1985); J. O. Fossum and K. Fosshem, *J. Phys. C* **18**, 5549 (1985).

¹²P. Wallace and C. W. Garland (unpublished).

¹³D. Durand, F. Denoyer, D. Lefur, R. Currat, and L. Bernard, *J. Phys. (Paris) Lett.* **44**, L207 (1983).

¹⁴The quantities $F(\omega\tau)$ and $G(\omega\tau)$ are identical to the functions $f(\omega\tau)$ and $g(\omega\tau)$ used in Table 7 of Ref. 11. These are related to the functions $f_\mu(\omega\tau)$ and $g_\mu(\omega\tau)$ used elsewhere in Ref. 11 by $F(\omega\tau) \equiv (zv/\mu\omega\tau)f_\mu(\omega\tau)$ and $G(\omega\tau) \equiv g_\mu(\omega\tau)$.

¹⁵B. Luthi and W. Rehwald, in *Structural Phase Transitions I*, edited by K. A. Müller and H. Thomas (Springer, Berlin, 1981).

¹⁶M. Barmatz, P. C. Hohenberg, and A. Kornbit, *Phys. Rev. B* **12**, 1947 (1975).

¹⁷W. Rehwald, *Adv. Phys.* **22**, 721 (1973).

¹⁸P. C. Hohenberg and B. I. Halperin, *Rev. Mod. Phys.* **49**, 435 (1977).

¹⁹R. A. Cowley and A. D. Bruce, *J. Phys. C* **11**, 3577 (1978); A. D. Bruce and R. A. Cowley, *ibid.* **11**, 3609 (1978).

²⁰I. Hatta and A. Ikushima, *J. Phys. Chem. Solids* **34**, 57 (1973).

²¹I. Hatta (private communication).

²²I. Hatta, *J. Phys. Soc. Jpn. Suppl.* **28**, 211 (1970).